Application of Autonomous Inflow Control Valve for Enhanced Bitumen Recovery by Steam Assisted Gravity Drainage

Soheila Taghavi[a,b], Farzan Farsi Madan[a] , Ramesh Timsina[a], Britt M. E. Moldestad[a]

[a] *Department of Process, Energy and Environmental Technology, University of South-Eastern Norway, Norway,*
[b]*InflowControl AS, Norway*
corresponding author: soheila.t.hosnaroudi@usn.no

Abstract

Steam assisted gravity drainage is a thermal method for enhanced bitumen recovery. In this method, steam is injected to bitumen and heavy oil to reduce the viscosity and make the oil mobile. However, early breakthrough of steam in some parts of the well results in loss of the required amount of steam in contact with the cold bitumen, and poor distribution of the steam chamber. This limits the oil production and increases the SAGD operation cost. Autonomous inflow control valve (AICV) is able to prevent the steam breakthrough and restrict the production of steam. The objective of this paper is to investigate the performances of AICV and passive inflow control device (ICD) in a SAGD production well. This is achieved by developing a dynamic wellbore-reservoir model in the OLGA-ROCX simulator. Reservoir and fluid properties have been specified in ROCX, and the wellbore model has been developed in OLGA. Coupling OLGA and ROCX enable the user to simulate the fluid production from the reservoir into the well. The simulation results demonstrate the significant benefit of AICV in steam to oil ratio (SOR) reduction compared to ICD. Indeed, the simulation results show that utilizing AICV in the SAGD production wells will reduce the steam production by 88% after 300 days of production. From environmental aspect, reduction in the steam to oil ratio by utilizing AICV will reduce the energy demand for steam generation. This will eventually improve the economics of SAGD projects. Also, reduction in the steam and energy demand will consequently contribute to lower the intensity of greenhouse gas (GHG) emissions.

1.Introduction

Steam assisted gravity drainage is a thermal recovery method based on gravity drainage for extraction of bitumen and heavy oil. More than 80% of the world's annual heavy oil production is by means of deploying this technology [1]. As the bitumen and heavy oil viscosity are as high as 10^6 cP, the mobility is very low. Thus, the viscosity must be reduced drastically to make the bitumen mobile and extractable. Therefore, the SAGD method is used, where the oil is heated to temperatures around 200°C and higher. At this temperature range, the oil viscosity is below 20 cP (see Figure 1) which implies that the oil is mobile and is able to flow towards the production well by gravity.

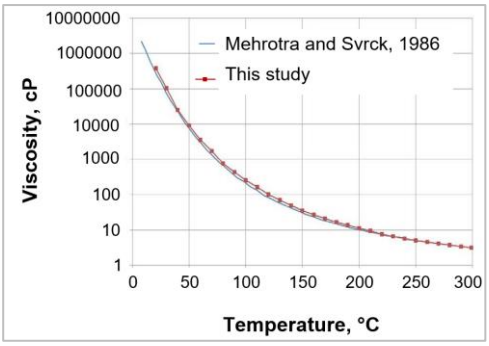

Figure 1:Viscosity of Athabasca bitumen sample versus temperature. [2]

The SAGD process is shown in Figure 2. Steam is injected continuously from the steam injection well which is located about 4-6m above the production well. As steam is injected, it forms a growing steam chamber with uniform temperature, called a depletion chamber. The continuous injected steam flows to the interface and condenses in contact with the cold bitumen. As a result, the latent steam energy is released leading to the higher oil temperature, lower oil viscosity, and consequently greater oil mobility. The low viscous mobile oil and condensate flow continuously from the edge of the steam chamber towards the production well.

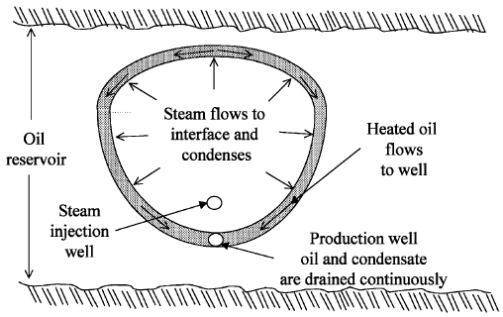

Figure 2:SAGD process. [3]

One of the key parameters of an efficient SAGD operation is attaining an even steam distribution

along the injection well. This can be achieved by deploying inflow control devices (ICDs) which balance the steam outflow to the reservoir. The role of ICD installation on the injection well is of great importance specially in the early phases of steam chamber growth, since it encourages more uniform steam development. [4]

One of the challenges in the SAGD wells is steam and water breakthrough in some parts of the well. This reduces the heavy oil/bitumen production and will consequently increase the SAGD operation cost. ICDs initially and autonomous inflow control devices (AICDs) latterly have been used to overcome this challenge. The newest generation of AICD is autonomous inflow control valve (AICV). AICV is able to delay the onset of steam and water breakthrough and ensure an even influx of oil along the well. In addition, in case of breakthrough of unwanted fluids like steam and/or water, AICV restricts the production of these fluids significantly. The ratio of steam injection to oil production (SOR) is of great importance in the SAGD process. From both environmentally and economically aspects, it is crucial to implement technologies which contribute to decrease the SOR.

The aim of this paper is to examine the impact of the ICD and AICV technology on reducing SOR and consequently improving the SAGD economics.

2. Inflow control technologies; ICD and AICV

Inflow control technologies such as ICDs and AICVs were introduced to the oil industry in order to overcome the early water and gas breakthrough challenges associated with heel-toe effect in horizontal wells. The heel-toe effect refers to the variations of the inflow rate of the fluid along the well, from toe to heel, due to the frictional pressure losses [5]. In addition, these technologies promote a balance drainage of long horizontal wells, and in general increase the oil production and recovery.

The following sub-sections present the functionality and performance curves of passive and autonomous inflow control device.

2.1. ICD

Figure 3 shows a pipe section with nozzle-type ICD completion. Fluid from the reservoir (red arrows) flows through the sand-screen, traverses along the annulus, and enters the production tubing through the ICD.

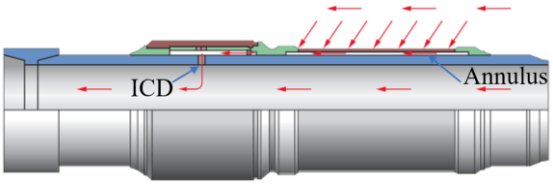

Figure 3: Nozzle-type ICD mounted on the pipe.[6]

The governing equation of the nozzle-type ICD is as follows [7]:

$$\Delta P = \frac{8\rho Q^2}{d^4\pi^2 n^2 {C_D}^2} \quad (1)$$

Where ΔP is the pressure drop through the nozzle, ρ is the fluid density, Q is the volumetric flow rate of the fluid through the nozzle, d is the diameter of the nozzle, n is the number of tested nozzles, and C_D is the discharge coefficient. C_D is mostly a function of the Reynolds number (Re) [7]. It can be interpreted from the equation (1) that the pressure drop through the nozzle is mainly dependent on the fluid density. The performance curve of a nozzle type ICD for water, oil and gas is shown in Figure 4. A nozzle type ICD with 4.75 mm diameter is used in the simulations. By performance curve, it means that the pressure drop through the device is plotted as a function of the volume flow rate of the fluid.

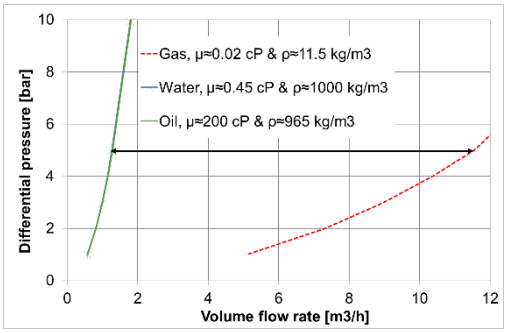

Figure 4: ICD performance curves.[8]

As it is illustrated in Figure 4, at constant pressure drop, the volume flow rate of oil and water differ slightly as the density differences are minor (1000 kg/m^3 for water vs 965 kg/m^3 for oil), while the volume flow rate of gas is much higher due to the much lower density (about 11.5 kg/m^3). This indicates that when gas breakthrough occurs, ICD will not restrict the gas production significantly.

2.1. AICV

Figure 5 shows a pipe section with sand screen and AICV completion.

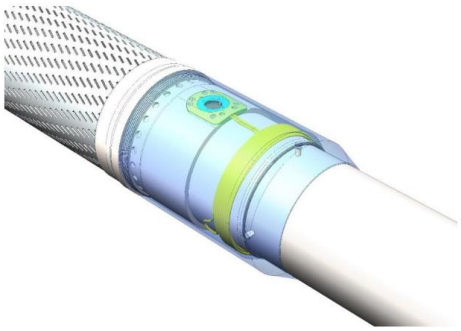

Figure 5:AICV mounted in a base-pipe with sand screen.[9]

The mathematical model describing the performance of the AICV can be described as:

$$\Delta P_{Tot} = \left(\frac{\rho_{mix}^2}{\rho_{cal}}\right) \cdot \left(\frac{\mu_{cal}}{\mu_{mix}}\right)^{y} \cdot a_{AICD} \cdot Q^{x} \qquad (2)$$

where ΔP_{Tot} is the differential pressure across the AICV, ρ_{cal} and μ_{cal} are the calibration fluid density and viscosity, and ρ_{mix} and μ_{mix} are the mixture fluid density and viscosity respectively. The parameter a_{AICD} is a valve characteristic given by the ICD strength, Q is the volumetric mixture flow rate, and x and y are constants. [10]

It can be interpreted from equation (2) that the pressure drop through the AICV is much more viscosity dependent than density dependent. The concept and principle of AICV is described in detail in earlier scientific works [11, 12].

The performance curve of AICV for water, oil and gas is shown in Figure 6.

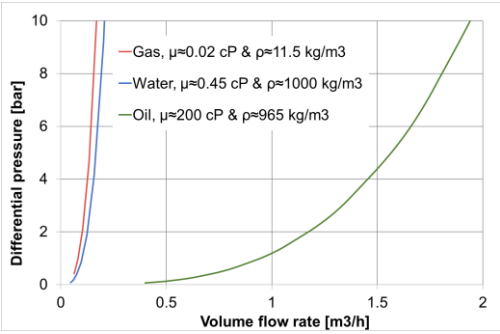

Figure 6:AICV performance curves.[8]

As it is illustrated in Figure 4 and Figure 6, at constant pressure drop the volume flow rates of oil with 200 cP viscosity through the ICD and the AICV are almost the same, while the gas flow rate is significantly higher through the ICD than the AICV. The location of performance curves of the gas and water for AICV have changed compared to the performance curves through ICD. The gas and water curve are now located far away to the left side of the oil curve. This indicates that when gas and water breakthrough occur, AICV will restrict the gas and water production significantly while maintaining a high oil production.

3. OLGA-ROCX set up

In this study, OLGA-ROCX is used to describe and compare the behavior of ICD and AICV in the SAGD reservoir, and to illustrate the impact of AICV completion on increased oil recovery. OLGA-ROCX is an integrated transient well/reservoir model. The reservoir model and the wellbore model are coupled in an implicit way [13]. Reservoir and fluid properties are specified in ROCX, and the wellbore model is developed in OLGA. Coupling OLGA and ROCX enable the user to simulate the fluid production from the reservoir into the well. NETool was used to simulate the AICV performance in a SAGD reservoir in previous author's work [8]. NETool is a static one-dimensional steady state simulation tool that shows the instantaneous inflow profile along the well, while OLGA/ROCX is a robust transient simulation tool to perform integrated well-reservoir simulations.

3.1. Reservoir model, ROCX

The black oil model which simulates the multiphase fluid transport in porous media is selected in ROCX. Input data to the model are grid dimensions, fluid, and reservoir properties. Reservoir properties such as permeabilities and porosities of the porous medium, and in addition thermal properties of the rock and fluids are among the input data. Initial conditions such as fluid saturations and temperature together with the boundary conditions at the well and at the outer near well boundary are needed. [14]

The boundary conditions of the reservoir grid elements are matched with inflow points of the components placed in the wellbore model. This will define the flow from the reservoir model. So, the pressure boundary for the reservoir model is provided by the wellbore model while the reservoir model provides the flow and the fluid temperatures into the pipeline[14]. The shape of the reservoir drainage area is considered to be rectangular, and the dimensions are given in Table 1.

Table 1:The dimensions of the drainage area.

Direction	Length (m)	Number of blocks	Block size (m)
X	1000	10	100
Y	117	15	20,20,5,5,3,3, 2,1,2,3,3,5,5, 20,20
Z	40	10	4

As the fluid properties varies significantly around the well and in the Y-Z plane, a finer mesh is considered in the grid setup to achieve more accurate results. The size of the blocks varies along the y direction while a uniform mesh along the z and x-direction is defined. Finer mesh along the x-direction will have insignificant impact on the overall flow rate [15]. The well length is 1000 m containing 10 segments with a length of 100 m each. One equivalent ICD/AICV is placed in each segment.

Since the purpose of this study is to evaluate the ICD/AICV performance in case of steam breakthrough, the well is located as near as possible to the bottom of the drainage area to delay the probable steam breakthrough. The schematic of the drainage area geometry and the well location is shown in Figure 7.

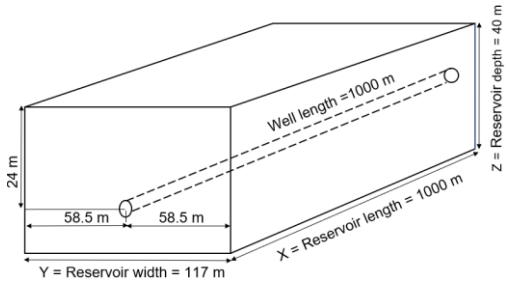

Figure 7:The schematic of the drainage area geometry.

The grid in three dimensions is shown in Figure 8.

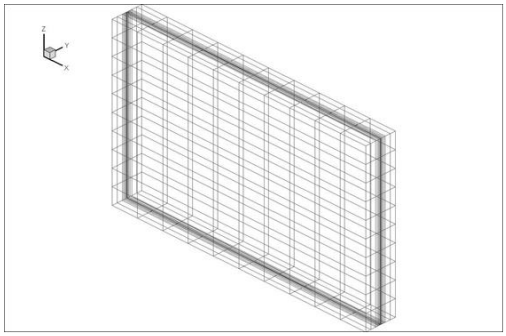

Figure 8:3-D view of grid.

As seen from the figure, the mesh in the y-direction and towards the well located in the middle of the drainage area is finer than in the z and x-direction.

3.1.1 Fluid and reservoir properties

The black oil model which estimates the pressure volume temperature (PVT) relations is selected in ROCX. The basic modeling assumption is that the gas may dissolve in the liquid oil phase, but no oil will dissolve in the gaseous phase. This implies that the composition of the gaseous phase is assumed the same at all pressure and temperatures [12],[16].In other words, the black oil model assumes that the oil components will always be in the liquid phase despite any changes in the conditions [15] .

The reservoir pressure at initial conditions is 27 bar and it is assumed to be constant. The fluid properties used for the simulation are listed in Table 2. The oil viscosity is measured at 180°C at atmospheric pressure [2].

Table 2: Fluid properties as input in ROCX.

Property	Value
Oil viscosity [cP]	15.50
Oil specific gravity [-]	0.90
Gas specific gravity [-]	0.64
Gas oil ratio (GOR) [Sm^3/Sm^3]	150

A gas cap is placed at the top of the reservoir in the boundary conditions section. Hence a gas feed in addition to oil feed are defined. The feed streams are presented in Table 3.

Table 3:Feed streams.

Feed stream	Fraction type	Fraction
Oil	GOR	150
Gas	OGR	0.99

The reservoir porosity is assumed to be constant 0.3 throughout the reservoir. Different permeabilities are specified for each block in order to simulate a heterogenous reservoir. It is assumed that the area close to the toe section of the well has a higher permeability in all directions. The permeability of the heterogenous reservoir in both x and y-direction, varies from 3000 mD in relatively low permeable zones to 6000 mD in relatively high permeable zones. The vertical permeability is specified in each block of the reservoir, and it varies from 300 to 600 mD for relatively low permeable and relatively high permeable zones respectively. The vertical permeability profile of the heterogenous reservoir is illustrated in Figure 9

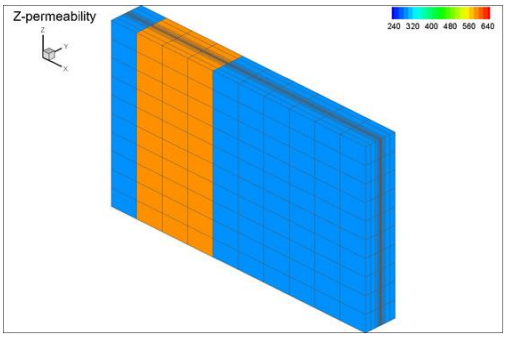

Figure 9:Vertical permeability profile.

Generally, it is challenging to obtain information about relative permeability for different fields. Data for relative permeabilities are set manually in table

form in Rocx. The "Stone II" model with exponent 2 is used to evaluate the oil phase relative permeability while the Corey correlation with exponent 1.5 is used to estimate the gas phase relative permeability. The relative permeability curves for oil and gas are presented in Figure 10.

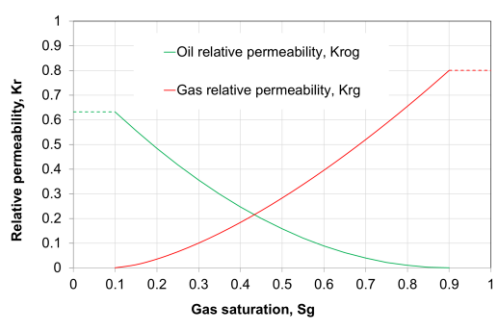

Figure 10: Relative permeability curves for the SAGD reservoir.

3.1.2 Initial and boundary conditions

Initially, it is assumed that the fraction of the black oil feed is equal to one. The initial oil and gas saturation of in the reservoir are set to 0.9 and 0.1. Pressure and temperature of the reservoir are 27 bar and 180°C, respectively.

3.2. Wellbore model, OLGA

In OLGA, separate continuity equations are applied for the gas, for the oil (or condensate) and water liquids and also for oil (or condensate) and water droplets. Three momentum equations are also used: one for each of the continuous liquid phases (oil/condensate and water) and one for the combination of gas with liquid droplets. One mixture energy equation is also applied. Totally, seven conservation equations and one equation of state to be solved: the seven conservation equations are three for mass, three for momentum, and one for energy, while the equation of state is for pressure.[17]

3.2.1 Mass Transport Equations:

$$\partial_t m_i + \partial_z(m_i U_i) = \sum_i \Psi_{ji} + G_i \qquad (3)$$

where m_i and U_i denote mass field (gas, oil in liquid layers, water in liquid layers, oil droplets in gas layer, and water droplets in gas layer) and velocity respectively. In addition, ∂_t denotes differentiation in time, ∂_z denotes spatial differentiation, Ψ_{ji} denotes the rate of mass transfer between the j-th and i-th mass field, that is, dispersions, droplet deposition and entrainment, and phase transitions, and G_i denotes any mass source/sink.

3.2.2 *Momentum Balance Equations*

$$\partial_t(m_i U_i) + \partial_z\left(m_i {U_i}^2\right) = m_i . g . \cos(\varphi) + \not{p}_i + G_i U_i + \sum_j \left(\Psi_{ji}^{+} U_i - \Psi_{ji}^{-} U_i\right) + \sum_j F_{ji}^{I}\left(U_j - U_i\right) - F_i^{w} U_i \qquad (4)$$

where ∂_t denotes differentiation in time, ∂_z denotes spatial differentiation. g is the acceleration of gravity, φ is the pipe angle relative to the gravitational vector, P_i is the pressure force, $G_i U_i$ is the momentum contribution corresponding to the mass source/sink G_i. Also, F^{I}_{ji} are friction forces between the i-th and j-th mass field, and F^{w} denotes the wall friction. Ψji denotes momentum contributions corresponding to the mass transfer between the j-th and i-th mass field. In the equation (4), Ψ^{+}_{ji} accounts for a net contribution from mass field i to j while Ψ^{-}_{ji} accounts for a net contribution from mass field j to i.

3.2.3 Energy balance equation

$$\partial_t(m_i E_i) + \partial_z(m_i U_i H_i) = \mathcal{S}_i + \mathcal{Q}_i + \sum_i T_{ij} E_j \qquad (5)$$

where E_i denotes the field energy, H_i denotes the field enthalpy, S denotes enthalpy source/sink, Q is the heat flux through the pipe wall, and T_{ij} models the energy transfer between fields.

3.3 OLGA set-up

In this work, a basic case is selected to generate the wellbore model in OLGA. The model consists of two pipes: pipeline and flowpath. The flowpath represents the production tubing, and the pipeline represents the annulus and the inflow from annulus to the well. On the pipeline, the flow components such as inflow controls and packers are placed. The characteristics and dimensions of the two pipes are listed in Table 4.

Table 4:The characteristics of pipeline and flowpath.

Pipe	Length (m)	Diameter (mm)	Roughness (mm)
Pipeline	1000	222	0.028
Flowpath	1000	114	0.050

Figure 11 shows the set-up in OLGA for one production zone which consists of two sections. This set-up was developed and proposed for the first time in 2012 [12] and results were presented in a scientific paper [11].

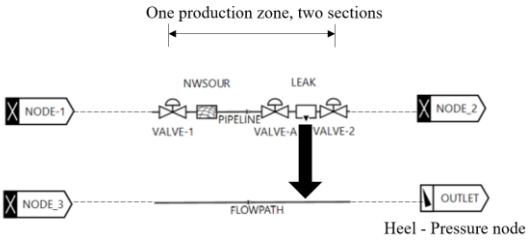

Figure 11:Set-up of a single production zone with inflow controller in OLGA.

The pipeline (PIPELINE) includes a near-well source (NWSOUR) which connects the ROCX file

as input data. The near-well source is the flow source from the reservoir to the annulus. In addition, the pipeline consists of one inflow controller (VALVE-A), two packers (VALVE-1 and 2 with zero opening), and leak (LEAK) which outflows the flow through the inflow control to the production well (FLOWPATH) and towards the heel (OUTLET). Each production zone is divided into two sections and is isolated by packers. The near-well source and the leak is placed in each section and the packers, and the inflow controllers are the section boundaries. Each pipe is divided into 10 production zones each 100 m long which implies that there are totally 20 sections.10 nozzle type ICDs with a diameter of 15 mm is distributed in the 10 production zones. The flow area of this ICD in one production zone (100 m) corresponds to the flow area of 10*4.75 mm ICDs. Usually, in the industry, the ICDs are installed in approximately 10-11 m long joints. So, the flow area of one equivalent ICD in a 100 m production zone is approximately the same as the flow area of 10 ICDs with 4.75 mm diameter which are installed in 10-11 meters long joints.

A comprehensive and step by step workflow for modelling of the rate controlled production (RCP) valves in the OLGA simulator was proposed in a scientific paper [18]. In this new method, a controller is used to chock the RCP valve based on the characteristics of the RCP valve and the reservoir fluid mixture. This method can also be used for AICVs. Set-up of a single production zone with AICV in OLGA is illustrated in Figure 12 .

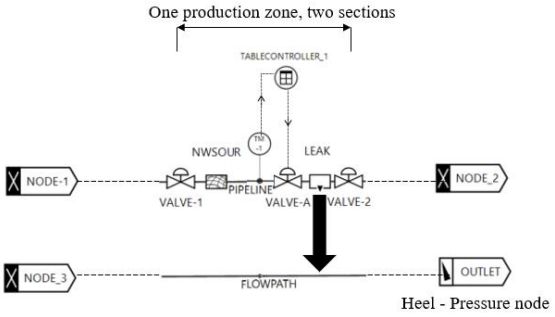

Figure 12:Set-up of a single production zone for AICV in OLGA.

Based on the single-phase (Figure 6) and multi-phase gas/oil performance of the AICV, a table controller (TABLECONTROLLER-1) is created. This table controller gets the measured gas volume fraction (GVF) data from the transmitter (TM-1) and provides corresponding control signals for chocking the AICV. The multiphase gas/oil behavior of the AICV for SAGD conditions was presented earlier in a scientific paper [8] . According to the experimental results provided in that paper, the AICV gradually opens when the oil/gas mixture flows through the valve. However, the AICV restricts the gas flow when the GVF is getting higher, until pure gas flows through the valve and the valve is almost closed.

The control signal table in the OLGA simulator for controlling the AICV, consists of independent and dependent variables. In this case, the percentage of the valve opening is a function of the GVF. Indeed, the valve opening is getting less and less by increasing the GVF.

4. Results and discussion

In this chapter, the obtained simulation results which are conducted for two cases are presented. The simulation cases are as follows:

1. Heterogeneous reservoir with ICDs
2. Heterogeneous reservoir with AICVs

The gas density and viscosity in the simulations performed by OLGA/ROCX, are set to 11.5 kg/m^3 and 0.02 cP respectively. In the simulations and the experiments, the gas represents steam.

In order to study the performance of ICD and AICV in a specific well production period, the accumulated oil and gas for AICV and ICD completions are compared. Figure 13 illustrates the accumulated oil and gas produced from the well after 300 days of production.

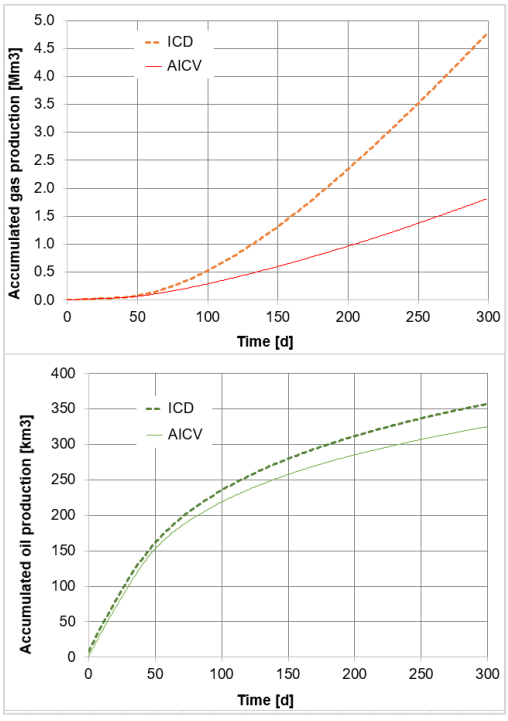

Figure 13:Accumulated oil and gas from the well completed with AICVs and ICDs.

As can be seen in this figure, after 300 days of production, the accumulated oil in the AICV and ICD cases differs marginally. However, due to the better performance of AICV in both single and multiphase flow regions, the amount of accumulated gas drops significantly from 4.8 Mm^3 to 1.9 Mm^3 after 300 days of production.

When the gas breakthrough occurs, AICV starts to chock the gas production gradually. Indeed, AICV chocks the gas production consistently by increasing GOR. This behavior, which is based on experimental data [8], was implemented in the Table Control module in OLGA.

Figure 14 Shows the comparison of oil and gas production rates for AICV and ICD completion for 300 days of production. The oil production rate for both cases reach its maximum at the start of the production. The oil production decreases slightly as the gas production increases simultaneously. Gas production grows suddenly and rapidly at 35th day of production, which implies that gas breakthrough has occurred. At the time of gas breakthrough, gas enters the well rapidly due to its high mobility. This restricts the production of oil significantly, and as a result, the oil production rate drops drastically. However, oil production is continued at an acceptable level until the end of the production time.

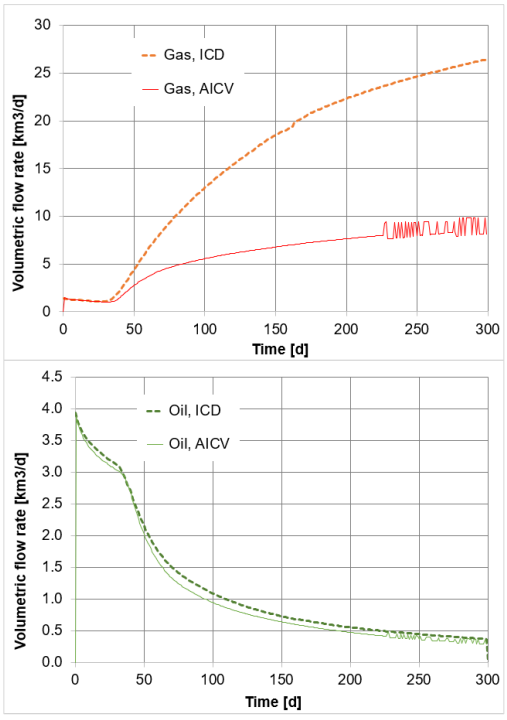

Figure 14:Voumetric flow rate of oil and gas for the well completed with AICVs and ICDs.

As can be seen from the figure, the volumetric oil flow rate of ICD is on average slightly higher than the volumetric oil flow rate of AICV during the whole period of production. However, the gas breakthrough occurs a few days later for the AICV case than for the ICD case. Also, the development of gas breakthrough is much faster for the ICD case compared to the AICV case. It can be concluded from the figure that the well completed with AICVs reduces the gas production by approximately 88% compared to using ICDs after 300 days of production.

Figure 15 shows the GOR at standard conditions as a function of accumulated oil production. This figure illustrates how the GOR varies with accumulated oil. Usually in the wells, the total allowable gas production is limited, since the total gas processing capacity is an active constraint [19]. This highlights the importance of developing new inflow control technologies which guarantee a higher maximum oil production while meeting the GOR constraint.

As it can be seen from the figure, the accumulated oil at a specific GOR, for example 600, for the AICV case is 15% more than the accumulated oil for the ICD case.

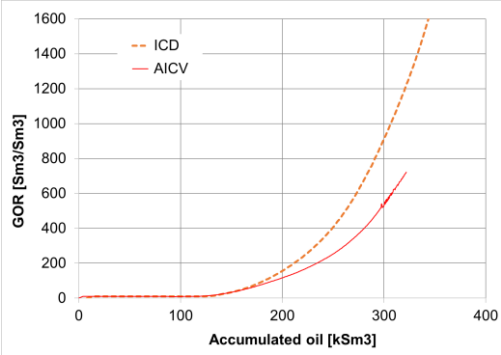

Figure 15: Accumulated oil production versus gas oil ratio for AICV and ICD.

4. Conclusions

The performances of AICV and ICD in a SAGD production well are investigated. This is achieved by developing a dynamic wellbore-reservoir model in the OLGA-ROCX simulator. Reservoir and fluid properties are specified in ROCX, and the wellbore model is developed in OLGA. Coupling OLGA and ROCX enable the user to simulate the fluid production from the reservoir into the well.

The simulation results demonstrate the significant benefit of AICV in SOR reduction compared to ICD. Indeed, simulation results show that utilizing AICV in the SAGD production wells will reduce the gas (steam) production by 88% after 300 days of production. Reduction in SOR, will improve the overall SAGD operation performance. This will also result in more cost-effective oil production.

From environmental aspect, reduction in the steam to oil ratio by utilizing AICV, will reduce the energy demand for steam generation. This will improve the economics of SAGD projects. Also, reduction in the steam and energy demand will consequently contribute to lower the intensity of greenhouse gas (GHG) emissions.

Acknowledgment

The author would like to thank the university of South-Eastern Norway for providing the necessary software arrangements for this work.

References

[1] Z. Xu, S. Li, B. Li, D. Chen, Z. Liu, and Z. Li, "A review of development methods and EOR technologies for carbonate reservoirs," *Petroleum Science*, pp. 1-24, 2020.

[2] A. Jahanbani, T. Jelmert, J. Kleppe, M. Ashrafi, Y. Souraki, and O. Torsæter, "Investigation of the Applicability of Thermal Well Test Analysis in Steam Injection Wells for Athabasca Heavy Oil," 06/04 2012, doi: 10.2118/154182-MS.

[3] R. Butler, "SAGD Comes of AGE!," *Journal of Canadian Petroleum Technology*, vol. 37, no. 07, 1998, doi: 10.2118/98-07-da.

[4] B. Least, S. Greci, R. Huffer, R. V. Rajan, and H. Golbeck, "Steam Flow Tests for Comparing Performance of Nozzle, Tube, and Fluidic Diode Autonomous ICDs in SAGD Wells," in *SPE Heavy Oil Conference-Canada*, 2014, vol. Day 3 Thu, June 12, 2014, D031S013R005, doi: 10.2118/170083-ms. [Online]. Available: https://doi.org/10.2118/170083-MS

[5] V. M. Birchenko, K. M. Muradov, and D. R. Davies, "Reduction of the horizontal well's heel–toe effect with inflow control devices," *Journal of Petroleum Science and Engineering*, vol. 75, no. 1, pp. 244-250, 2010/12/01/ 2010, doi: https://doi.org/10.1016/j.petrol.2010.11.013.

[6] T. Jokela *et al.*, "Inflow Control Devices — Raising Profiles," 2010.

[7] J. E. Lauritzen and I. B. Martiniussen, "Single and Multi-phase Flow Loop Testing Results for Industry Standard Inflow Control Devices," in *SPE Offshore Europe Oil and Gas Conference and Exhibition*, 2011, vol. All Days, SPE-146347-MS, doi: 10.2118/146347-ms. [Online]. Available: https://doi.org/10.2118/146347-MS

[8] S. Taghavi, H. Aakre, and B. M. E. Moldestad, "Performance Analysis of Autonomous Inflow Control Valve in a SAGD Late Life Process with Non-Condensable Gases," in *SPE Canadian Energy Technology Conference*, 2022, vol. Day 1 Wed, March 16, 2022, D011S011R002, doi: 10.2118/208915-ms. [Online]. Available: https://doi.org/10.2118/208915-MS

[9] H. Aakre, V. Mathiesen, and B. Moldestad, "Performance of CO2 flooding in a heterogeneous oil reservoir using autonomous inflow control," *Journal of Petroleum Science and Engineering*, vol. 167, pp. 654-663, 2018/08/01/ 2018, doi: https://doi.org/10.1016/j.petrol.2018.04.008.

[10] S. Taghavi and A. Ghaderi, "On Uncertainty Analysis of the Rate Controlled Production (RCP) Model," in *First SIMS EUROSIM Conference on Modelling and Simulation*, Finland, 2021: Linköping Electronic Conference Proceedings, 2021.

[11] H. Aakre, B. Halvorsen, B. Werswick, and V. Mathiesen, "Smart Well With Autonomous Inflow Control Valve Technology," in *SPE Middle East Oil and Gas Show and Conference*, 2013, vol. All Days, SPE-164348-MS, doi: 10.2118/164348-ms. [Online]. Available: https://doi.org/10.2118/164348-MS

[12] H. Aakre, n. o. m. f. Høgskolen i Sørøst-Norge Fakultet for teknologi, and S.-N. Høgskolen i, "The impact of autonomous inflow control valve on increased oil production and recovery," no. 32, University College of Southeast Norway, Faculty of Technology, Natural Sciences and Maritime Sciences, Kongsberg, 2017.

[13] G. Chupin, B. Hu, T. Haugset, J. Sagen, and M. Claudel, "Integrated Wellbore/Reservoir Model Predicts Flow Transients in Liquid-Loaded Gas Wells," in *SPE Annual Technical Conference and Exhibition*, 2007, vol. All Days, SPE-110461-MS, doi: 10.2118/110461-ms. [Online]. Available: https://doi.org/10.2118/110461-MS

[14] J. Sagen, T. Sira, A. Ek, S. Selberg, M. Chaib, and H. Eidsmoen, "A Coupled Dynamic Reservoir and Pipeline Model – Development and Initial Experience," in *13th International Conference on Multiphase Production Technology*, 2007, vol. All Days, BHR-2007-G1.

[15] N. C. I. F. Ramesh Timsina, Britt M. E. Moldestad, "Modeling and simulation of light oil production using inflow control devices," in *58th Conference on Simulation and Modelling (SIMS 58) Reykjavik, Iceland*, 2017: Linköping Electronic Conference Proceedings doi: http://dx.doi.org/10.3384/ecp17138180.

[16] "Black-Oil Simulations." wikitext. https://dwsim.org/wiki/index.php?title=Black-Oil_Simulations (accessed.

[17] K. H. Bendlksen, D. Malnes, R. Moe, and S. Nuland, "The Dynamic Two-Fluid Model OLGA: Theory and Application," *SPE Production Engineering*, vol. 6, no. 02, pp. 171-180, 1991, doi: 10.2118/19451-pa.

[18] A. Moradi and B. M. E. Moldestad, "A Proposed Method for Simulation of Rate-Controlled Production Valves for Reduced Water Cut," *SPE Production & Operations*, vol. 36, no. 03, pp. 669-684, 2021, doi: 10.2118/205377-pa.

[19] A. Mjaavatten, R. Aasheim, S. Saelid, and O. Groenning, "A Model for Gas Coning and Rate-Dependent Gas/Oil Ratio in an Oil-Rim Resevoir," in *SPE Russian Oil and Gas Technical Conference and Exhibition*, 2006, vol. All Days, SPE-102390-MS, doi: 10.2118/102390-ms. [Online]. Available: https://doi.org/10.2118/102390-MS